IRANIAN JOURNAL OF CATALYSIS

Enhancing the Photocatalytic Performance of TiO_2 Nanoflower Thin Films under Ultraviolet Irradiation

Marwah Jawad Kadhim[a*]; Mazin Auny Mahdi[a,*]; Jalal Jabar Hassan [a]

a) Department of Physics, College of Science, University of Basrah, Basrah, Iraq

Received 7 June 2023; received in revised form 21 September 2023; accepted 14 October 2023 (**DOI: 10.30495/IJC.2023.1988200.2011**)

ABSTRACT

Chemical bath deposition (CBD) was used to prepare titanium dioxide (TiO_2) nanocrystalline thin films on glass substrates. The TiO_2 nanocrystalline thin films were created, and the Scanning Electron Microscope (SEM) images showed that they developed as nanoflowers and tiny semi-nanoplate bundles that grew vertically onto the surface of the substrates with uniform distribution. The nanoplate ranges in length from 26 to 149 nm and the average thickness was between 13 and 228 nm. The prepared TiO2 nanoflower thin films have an energy band gap of 3.26 eV, according to optical characteristics. Using various pH values and UV light exposure durations, the photocatalytic activity of the produced TiO_2 nanoflower thin films was examined against the methylene blue (MB) dye at room temperature. When irradiation duration and pH were increased, the photodegradation rate of MB dye also increased. After 240 minutes of exposure, the photodegradation rate of MB dye with pH values of 6, 8, 9, 10, and 11 was 51%, 64%, 79%, and 82%, respectively. The kinetic rate constant for photocatalytic degradation of MB dye was determined to be 0.0069, 0.0061, 0.0038, and 0.0028 min^{-1} for pH values of 11, 9, 8, and 6, respectively.

***Keywords**: Photocatalyst, Nanostructures, TiO_2, Thin films, UV irradiation*

1. Introduction

The wastewater textile sector contaminated with dyes has become a serious concern in recent years owing to the varied composition of refractory pollutants, and it is difficult to treat. Every day, the textile industry, which employs dyes for color, consumes a large amount of freshwater [1]. Dyes and their intermediates can undergo oxidation, hydrolysis, and other chemical processes that could result in the production of potentially hazardous byproducts [2]. Dyes are organic chemicals that can be absorbed by, reacted with, or deposited within a substrate to give it color. In addition, a dye is a colorful and hazardous material [3]. Additionally, due to their toxicity, dye effluents can jeopardize both human and animal life. As a result, the majority of these colors are poisonous and carcinogenic, endangering aquatic life, microbes, and human health [4]. Methylene blue (MB) is one of the most often identified colors in textile effluent; it is very hazardous and may accumulate in different habitats [5-7]. Also, being a significant pollutant, it may cause harm to animals and other organisms and is primarily responsible for irreparable eye damage in humans [8]. One of the most serious issues confronting the human living system is the removal of organic contaminants from wastewater [9]. Treatment methods are increasingly important now. Researchers have developed several tactics for purifying contaminated water, including electrolyte decomposition, adsorbent addition, biological, ion exchange, sedimentation, coagulation/flocculation, steam stripping methods, etc. These purifying techniques are never an option at a large scale due to the high cost, thus alternative strategies are required, which are also dependable as green concoctions in nature. Photocatalysis allows for the green degradation of a wide range of organic contaminants. As a result, photocatalysis is regarded as a reliable innovation for the purification of contaminated water [10, 11]. Advanced oxidation procedures (AOP) are a form of chemical treatment that uses oxidation to remove organic colors from

*Corresponding author:
E-mail address: *marooj2013@gmail.com* (**M. J. Kadhim**); *m.a.mahdi@uobasrah.edu.iq* (**M. A. Mahdi**)

wastewater [12]. AOPs are influenced by the creation of highly oxidizing free radicals able to mineralize organic molecules, hence limiting the formation of waste products [13]. On the other hand, AOP is a process that uses up a lot of chemicals, and high treatment costs are one of the biggest reasons why it can't be used on a large scale [13]. Hydrogen peroxide, ozone, Fenton, cavitation, and photocatalysis were all methods of AOP [14]. AOP is based on the generation of powerful/non-selective hydroxyl and superoxide radical oxidants while irradiating a material of metal-oxide with adequate energy from UV or visible photons [15]. However, two main issues have been found regarding the use of hydroxyl radical-based AOPs in the treatment of landfill leachates. Firstly, the enhancement in the biodegradability of leachate exhibits a significant deficiency. Hence, it may be concluded that AOPs may not be a viable choice for pre-treatment in the context of biological treatment. Additionally, it is challenging for hydroxyl radical-based AOPs to effectively eliminate ammonia nitrogen, which is a significant pollutant found in leachate [16, 17]. Under UV irradiation, photocatalytic techniques utilizing semiconductors as photocatalysts [18] such as ZnO [19], WO_3 [20], CdS [21], and TiO_2 [22] have been widely used for the oxidation of different refractory organic dyes such as MB. Despite this, TiO_2 has been widely employed as a photocatalyst for dye degradation due to its strong photocatalytic activity, nontoxicity, chemical stability, photostability, and economic viability [14, 23]. The energy gap of TiO_2 in the anatase phase is equal to 3.2 eV, therefore it is photoactive in the UV region ($\lambda <$ 388 nm), and its application is limited by a very poor response to visible light [24]. The UV band has accounted for 3-5% of total solar energy used. The low fraction of photocatalysts that use solar light is owing to their low energy efficiency [25]. Furthermore, the high recombination rates of photo-induced charge carrier pairs in TiO_2 photocatalysts restrict their efficacy, making photocatalyst development critical [25]. So, TiO_2's photocatalytic activity against various dyes might be improved by the preparation of its distinct nanostructures. The recombination of photogenerated pairs can lead to a notable decrease in the overall effectiveness of the photodegradation process. The overall impact of the above processes is dependent upon the quantity of electron-hole pairs created. Consequently, many methodologies have been implemented to mitigate the extent of electron-hole recombination. The nano-sized approach significantly decreases the path length for photoinduced electron-hole (e-/h+) pairs to go from the bulk of the semiconductor to the surface. As a result, the (e^-/h^+) pairs exhibit enhanced migration towards the surface. Consequently, they are capable of engaging in the photodegradation process before undergoing recombination. Another method involves the introduction of metals and nonmetals into semiconductors, leading to the emergence of unique energy levels within the systems. Consequently, e^-/h^+ pairs that are generated by the absorption of photons in the conduction band (C_B) and valence band (V_B) of the primary semiconductor have the ability to move toward these newly formed energy levels. As a consequence, the recombination of e/h pairs reduces gradually over a period of time [26]. Titanium dioxide (TiO_2) exhibits various limitations that limit its optimal utilization in terms of photoefficiency. These downsides include a low surface area, poor adsorption capabilities, a limited ability to absorb sunlight, quick recombination of charge pairs, and difficulties in separating the components. These constraints significantly restrict the full potential of TiO_2 in achieving high photoefficiency. The reduced photoactivity of supported TiO_2 is often attributed to the interaction between TiO_2 and the support during thermal treatments. Therefore, it is crucial to improve the efficiency of photocatalysts, and there are various methods to achieve this objective. One such approach involves enhancing the structural morphology of the compound, such as creating unique shapes like nanoflowers. This modification can effectively increase the surface area, consequently leading to a higher rate of electron-hole recombination [27]. The current work used the chemical bath deposition (CBD) approach to create TiO_2 nanoflower thin films on glass substrates. The photocatalytic capabilities of the TiO_2 nanoflower thin films were evaluated against methylene blue (MB) dye and examined at different pH values and UV exposure durations.

2. Experimental

2.1 Preparation and characterization of TiO_2 nanoflowers thin films

The preparation of TiO_2 nanocrystalline thin films was carried out using the technique of chemical bath deposition (CBD), as described in previous studies [28, 29]. In summary, the initial step of the preparation procedure involves the utilization of an ultrasonic cleaner to cleanse glass substrates. This process involves placing the substrates to a 10-minute treatment utilizing a mixture of 2-propanol and ethanol. The substrates were then immersed in a beaker filled with a precursor solution consisting of 4 ml of titanium (III) chloride ($TiCl_3$) solution (15wt.% in HCl; Merck), 50 ml of deionized water (DI), and 0.1M of urea [NH_2CONH_2]

to achieve a pH level of about 0.5. After being stirred at room temperature for one hour, a uniform violet solution was formed. To fabricate TiO_2 nanocrystalline thin films, the substrates were immersed in the previously indicated solution in a vertical orientation. The temperature of the solution was then raised to 55 °C and maintained for 3 hours. Subsequently, the samples were extracted from the container and subjected to a series of rinses using distilled water (DW) and subsequently dried using air gas. To enhance the crystallinity, the TiO_2 nanocrystalline thin films are heated up to a temperature of 350 °C for one. **Fig. 1** is a schematic of the procedure for preparing TiO_2 nanocrystalline thin films. Field-Emission Scanning Electron Microscopy (FESEM) type NanoNova 450, FEI, The Netherlands; and X-ray diffraction analysis (XRD) (X'Pert PRO MPD with CuK radiation, PANalytical, The Netherlands) were used to examine the surface morphology and crystalline structure of the TiO_2 nanocrystalline thin films. A Shimadzu UV-vis spectrophotometer model UV-1800 was used to conduct the optical absorption.

2.2 Mechanism of TiO_2 Preparation via CBD Method

The CBD technique is an easy process that may be used to prepare multiple semiconducting nanocrystalline thin films on different substrates. In this process, nucleation sites on the substrate that is in contact with the chemical bath containing the precursor solutions result in the deposition of the thin film by an ion-by-ion mechanism [30]. According to the reaction below, titanium trichloride ($TiCl_3$) dissolved in HCl can be utilized as a source of titanium ions and ammonium chloride (NH_4OH) as a complexing agent.

$$TiCl_3 \longrightarrow Ti^{3+}+3Cl^- \quad (1)$$

$$NH_2CONH_2+3H_2O \longrightarrow CO_2+2NH_4OH \quad (2)$$

$$NH_4OH \longrightarrow NH_3+H_2O \quad (3)$$

The process below describes how the Ti^{3+} cations form an amine complex with ammonia to create $[Ti(NH3)_n]^{3+}$ in an aqueous solution.

$$Ti^{3+}+nNH_3 \longrightarrow [Ti(NH_3)_n]^{3+} \quad \text{(where n=1-4)} \quad (4)$$

However, $[Ti(NH_3)_n]^3$ is unstable and dissolves in the reaction shown below.

$$[Ti(NH_3)_n]^3 \longrightarrow Ti^{3+}+nNH_3 \quad (5)$$

The Ti^{3+} ion can be reacted with H_2O as below:

$$Ti^{3+}+nH_2O \longrightarrow [Ti(OH)_3]^+ \quad (6)$$

$$[Ti(OH)_3]^+ + OH^- \longrightarrow TiO_2+2H_2O \quad (7)$$

The pH level is a crucial factor that influences the development of TiO_2 nanocrystalline thin films; it should be between 0.5 and 0.7, since raising it may cause TiO_2 to precipitate out quickly without first forming a film [31]. At pH 2.5, TiO_2 precipitated quickly, but no film developed; by contrast, pH < 1.0 produced neither a precipitate nor a film [32].

2.3 Measurements of photocatalytic activity

When UV light illuminates the TiO_2 thin film photocatalyst, photoelectrons escape the valence band (VB) toward the conduction band (CB), leaving holes (h+). The holes in VB react with OH^- or H_2O adsorbed on the TiO_2 surface to make hydroxyl radicals, whereas the photoelectron in CB reacts with oxygen atoms to form superoxide radicals. These reactive can be written as follows [33, 34]:

$$TiO_2 + hv \rightarrow TiO_2(e_{CB}^-, h_{VB}^+) \quad (8)$$

$$h_{VB}^+ + OH_{ads.}^- \rightarrow OH^\circ \quad (9)$$

$$h_{VB}^+ + H_2O_{ads.} \rightarrow OH^\circ + H^+ \quad (10)$$

$$e_{CB}^- + O_2 \rightarrow O_2^{\circ -} \quad (11)$$

TiO_2 nanoflower thin films were produced on glass substrates and tested for their photocatalytic activity against MB dye as shown in **Fig. 2** which represented the mechanism of the photocatalytic process. The dye solution was prepared by dissolving MB dye at a concentration of $5x10^6$ g/ml in DW and adjusting the pH with drops of NaOH and HNO_3 acid solutions allowing for precise regulation of the dye solution's pH within the desired range of 6–11. However, the pH value is what determines the surface charge of the photocatalytic substance [35]. TiO_2 nanoflower thin films (2x2 cm) are submerged horizontally in 40 ml of MB solution and subjected to UV light irradiation at 265 nm for 240 minutes at several pH values to determine the photocatalytic activity of the produced samples.

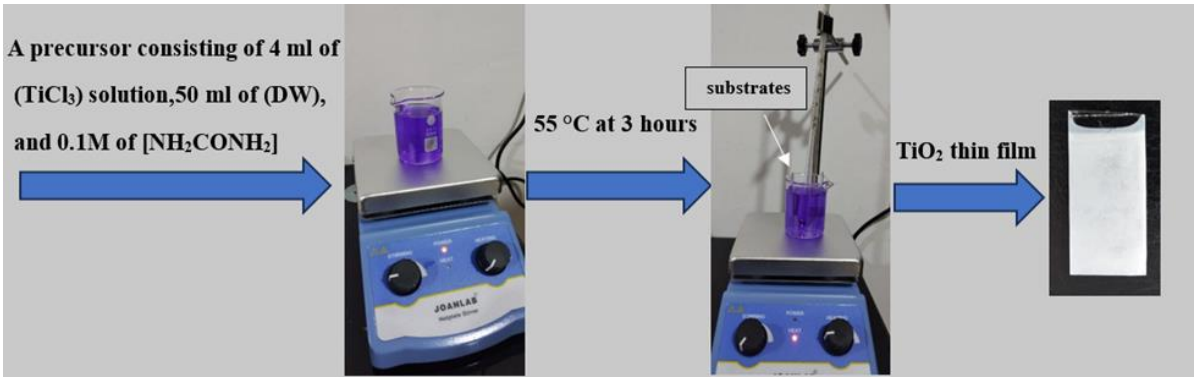

Fig. 1. Schematic of preparation of TiO_2 nanocrystalline thin films procedure

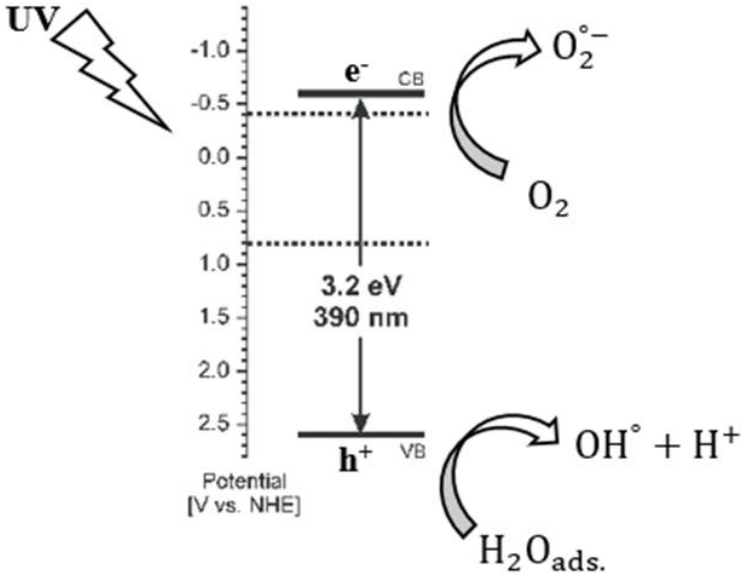

Fig. 2. Photocatalytic process mechanism of TiO_2 nanoflowers thin film under UV irradiation.

3. Results and Discussion

3.1 Morphological Study

Fig. 3 shows the images of the nanocrystalline thin films of TiO_2 nanoflower prepared on glass substrates using the CBD method. Thin films of TiO_2 that have been prepared are grown in the shape of nanoflowers. Also, each nanoflower was made up of small bundles of semi-nanoplates that grew vertically on the surface of the substrate. The average length of these bundles was between 26 and 149 nm, and the average thickness was between 13 and 228 nm.

3.2 Structure characterizations

Fig. 4 A shows the X-ray diffraction (XRD) pattern of TiO_2 nanoflowers. The standard database says that the XRD peaks are at diffraction angles (2) of 25.4°, 37.8°, 38.7°, and 48.1°, which are the same as anatase crystal planes (101), (004), (112), and (200) according to JCPDS Card no. 00-021-1272. Also, other XRD peaks showed up at 40.5°, which is the same as (110) crystal planes of the rutile phase (JCPDS Card no. 00-021-1276) [25]. But, even though the thin films of TiO_2 nanoflowers that were grown were heated, the crystallinity is still low. The crystalline size (D) was calculated according to the Debye-Scherrer formula :[36, 37]

$$D\ (nm) = \frac{k\lambda}{\beta \cos\theta} \qquad 12$$

where K is the incident Scherer constant, β is the FWHM diffraction peak, λ is wavelength X-ray, and θ the angle between the incident beam and crystal plane. The crystalline size value is 98.12 nm of the TiO_2 nanoflower thin films. While crystalline size is 77.90 nm by the Williamson-Hall (W-H) model calculated from the same sample according to the equation following [38].

$$\frac{\beta \cos\theta}{\lambda} = \frac{1}{D\ (nm)} + \frac{\varepsilon \sin\theta}{\lambda} \qquad 13$$

Particle size D represented the inverse of the y-intercept on the axis as shown in **Fig. 4B**.

3.3 Optical properties

The produced TiO_2 nanoflower thin film absorbance spectra are shown in **Fig. 5A**. The absorption edge is seen in the UV region at a wavelength of about 380 nm. Using the Tauc's relationship following [39], [40]:

$$\alpha h\nu = A(h\nu - E_g)^n \qquad 14$$

where, α, hυ, A, Eg, and n are the absorption coefficient, the incident photons energy, the constant absorption, the band gap, and the transition type (direct, forbidden direct, indirect, and forbidden indirect), respectively. The transition type of direct is 1/2, forbidden direct is 3/2, indirect is 2, and forbidden indirect is 3 [41]. In addition, the absorption coefficient is ([2.303x Abs.]/D) according to beer-lambert low, where Abs and D are the absorbance of the sample and thickness, respectively [42].

It was determined that the energy gap of TiO_2 nanoflower thin films is 3.26 eV, as shown in **Fig. 5B**. A.H. Mayabadi et al. [32] created mixed rutile and anatase structures with an energy band gap of 2.29 eV by growing TiO_2 nanocrystalline thin films onto glass surfaces using CBD at R.T and pH values of 0.5 to 1.5 for 25 hours. J.M. Kalita et al. [43] used the CBD approach to manufacture TiO_2 nanocrystalline thin films on glass substrates for 2 hours at 80 °C. The resultant films had an anatase phase and an optical band gap of 3.26 eV.

3.2. Photodegradation of MB dye

The optical absorbance under UV light irradiation and different pH values were used to evaluate the rate of MB

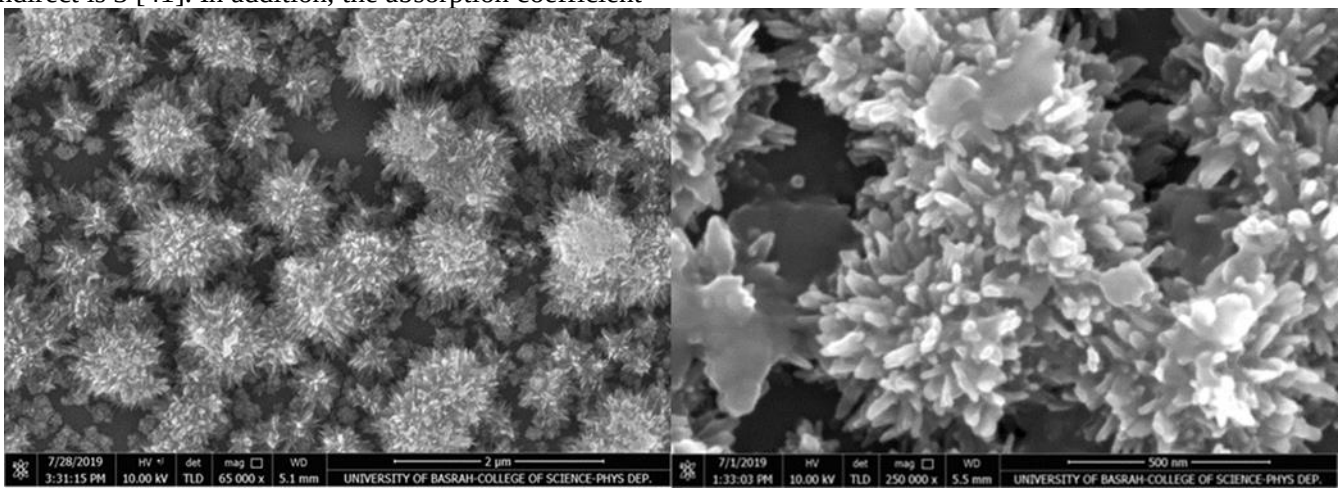

Fig.3. Various magnification of FE-SEM images of prepared TiO_2 nanoflowers thin films

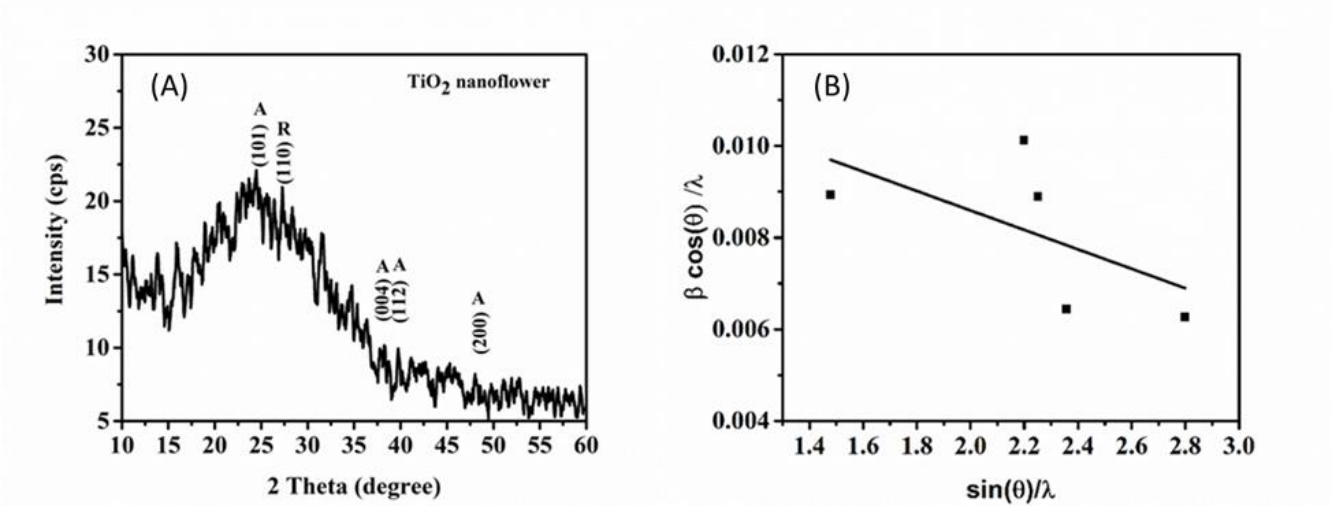

Fig.4 (A) X-ray diffraction spectra and (B) W–H plot of TiO_2 nanoflowers thin films grow on the glass substrate.

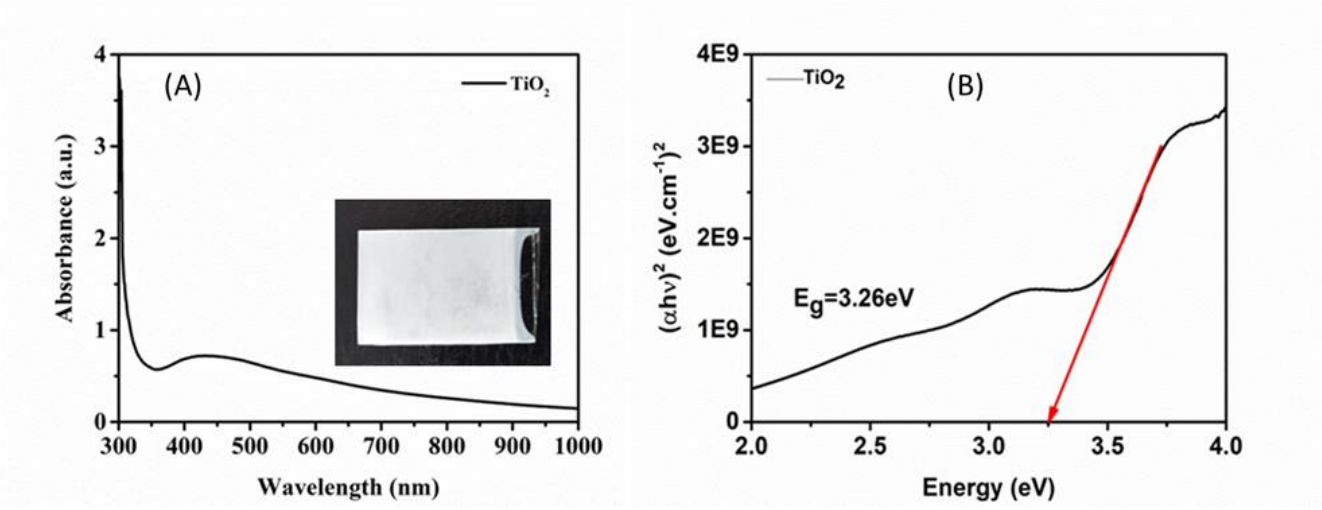

Fig.5. (A) The absorbance spectrum and (B) the plot of $(\alpha h\upsilon)^2$ versus photon energy of TiO_2 nanoflowers thin films grow on the glass substrates.

dye degradation caused by the TiO_2 nanoflower thin films photocatalyst, as shown in **Fig. 6**. In **Fig. 6D**, the absorbance spectra of the MB dye treated by TiO_2 nanoflower thin films as a photocatalyst under UV light irradiation are displayed. The exposure periods ranged from 30 to 240 minutes, and the pH values ranged from 6 to 11. As can be seen in **Fig. 6A-D**, the photodegradation efficiency of the TiO_2 nanoflower thin-film photocatalysts increases as exposure duration is increased for different pH values. The absorbance of MB dye treated with TiO_2 nanoflower thin films at pH 6 is shown in **Fig. 6A**, and it is seen that the absorbance decreases with longer illumination times. The literature extensively covers the decolorization of photocatalytic dyes, which is believed to include the generation of OH° radicals through a range of mechanisms. The radicals proceed to engage in an aggressive interaction with the dye molecules, resulting in their progressive degradation and elimination, as depicted in equation (8-11). The cleavage of one or more methyl group substituents on the amine groups leads to intermediate products with masses that agree with the eluted intermediates. The literature has documented the synthesis of azures and thionin through demethylation cleavage during degradation [44]. Based on the results, **Fig. 6 A-C** noted molar absorbancy of the MB dimer for a longer time of the monomer peak this is due to the molar absorption of dimer MB having more than the monomer of dye. This validates the dimer's increased resonance and stability for eliminating its intermediates [45]. **Fig. 6D** could confirm that the monomer photodegrades more quickly than the MB dimer. This phenomenon may be thought of as a virtual equilibrium phase of dimer formation in the presence of photons [46].

The photodegradation ratio of the MB dye was calculated using the formula [19]:

$$Degradation\ rate(\%) = \frac{A_{\circ}-A}{A_{\circ}} \times 100, \qquad 15$$

where A_o, *and* A represent the absorbance value before and after exposure, respectively.

The relationship between MB dye degradation rate and exposure duration for TiO_2 nanoflower thin films is seen in **Fig. 7**. All MB dye solutions prepared with various pH values have a photodegradation rate that rises with increasing irradiation time. When the duration was increased from 30 to 240 minutes, the degradation rate went from 31% to 51%. Additionally, within the same time frame, the degradation ratio jumped from 23% to 64% when the dye solution's pH was 8. The degradation rate reached 79% after 240 minutes of light for pH 9, which exhibits the same behavior. The maximum degradation ratio of 82% was attained at a pH of 11 and 210 minute exposure duration. Additionally, at illumination times of less than 120 minutes, the degradation ratio of MB dye increased by almost three times when the pH raise from 6 to 11. This phenomenon is explained by an increase in the concentration of a substance that interacts with photogenerated pores in water to oxidize organic contaminants like MB dye [47]. Furthermore, surface oxygen vacancies may be related to catalytic efficacy for TiO_2 and Ti vacancies, which are highly unsaturated and operate as catalytic sites. Furthermore, TiO_2 is n-type and contains oxygen vacancies, and Ti vacancies, which are associated with high energy and ensure that electrons are transferred from the valence to the conduction band. The oxygen vacancies occur often, but not always in couples with

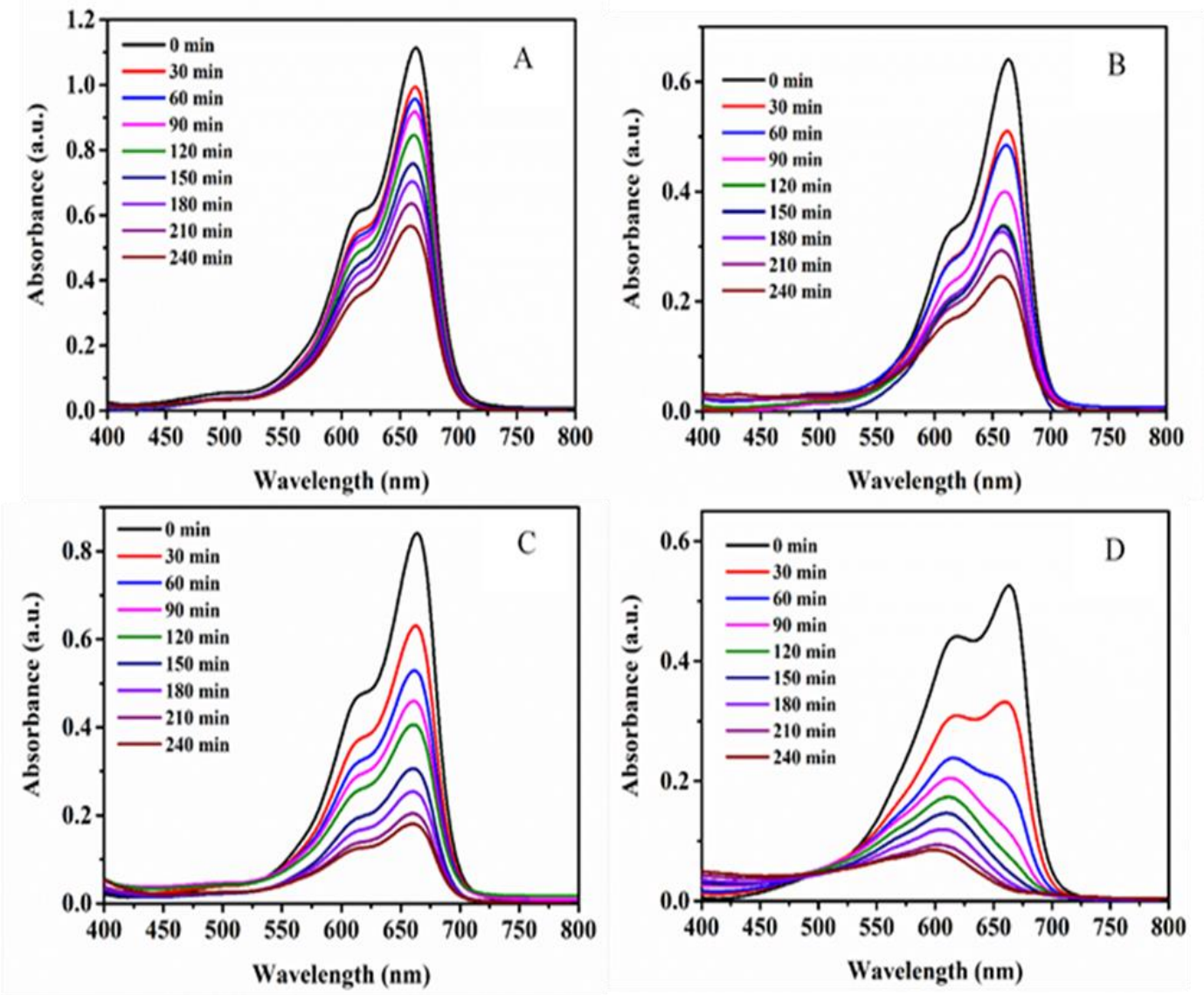

Fig.6. Absorbance spectra of MB dye treated by TiO_2 nanoflowers thin film for different UV irradiation times and various pH values of (A) 6, (B) 8, (C) 9, and (D) 11

neighboring Ti vacancies, and the adsorbed oxygen molecules can facilitate vacancy diffusion. It is no longer essential to deposit the electrons corresponding to Ti in the conduction band if the surface oxygen vacancies and surrounding Ti are eliminated. That is, the presence of adjacent Ti vacancies stabilizes the oxygen vacancies [48]. Al-Shamali [49] reported a photodegradation rate of 90% of MB dye in TiO_2 photocatalyst with pH values ranging from 4 to 8. A comparable study was undertaken by several other researchers, as shown in **Table 1**.

Because of the substantial pH dependence of features such as semiconductor surface charge state and chemical dissociation in solution, the pH of the solution influences photodegradation processes. Because of the existence of more hydroxyl radicals in the solution, a larger degradation extent would be expected at strong basic pHs. [16].

A more comprehensive understanding of the relationship between pH value and photodegradation efficiency can be achieved by determining the point of zero charges (PZC) [50]. Nevertheless, it should be noted that the catalyst's surface exhibited a negative charge when the pH value exceeded the point of zero charge (pHzpc), conversely, a positive charge was observed when the pH value was lower than the pHzpc. Additionally, the catalyst's surface remained electrically neutral when the pH value was almost equal to the pHzpc [51-53]. In other meaning, prevented the repulsion of columbic adsorption of ion hydroxide to the surface catalyst [54]. Some dyes degrade on the photocatalyst surface, where dye adsorption is an

important step in the process of photocatalytic degradation. Despite the fact that a dye with a high adsorption rate fades quickly, the number of UV light absorption impact sites reduces as adsorption rises [55].

The first-order Langmuir relation is described by the kinetics rate of the MB dye by the following formula [19]:

$$C = C_o e^{-kt} , \qquad 16$$

where C_o and C are the starting concentrations of the MB dye before and after light exposure, respectively, t is the reaction period, and k is the photodegradation reaction kinetics rate. The kinetic behavior has been widely utilized to assess the kinetics of a typical photocatalytic heterogeneous process based on the adsorption monolayer of products at the interface of solid-liquid and reactants. The adsorption described here is a process of equilibrium in which the adsorption amount of each of the reductants, and oxidants influences the photodegradation process of the contaminant and its intermediates of degradation. Furthermore, the adsorption of these compounds on the catalyst surface determines the rate of the photodegradation process total [56]. However, the adsorption of the pollutant and the oxidant is a critical kinetic parameter in the photodegradation process a heterogeneous. In addition, the Langmuir-Hinshelwood model is used to describe the kinetic behavior of degradation, but only when equilibrium of the photodegradation process [41].

Fig. 8 depicts the fluctuation of ln (C/C_o) vs. irradiation duration for TiO_2 nanoflower thin films with varied MB dye solution pH levels. For pH values of 11, 9, 8, and 6, the kinetic rate derived using the slope of Fig. 7 is 0.0069, 0.0061, 0.0038, and 0.0028 min^{-1}, respectively. **Table 2** presents degradation rate and kinetic rate measurements acquired every 30 minutes. S. Rajagopal et al. [14] discovered that the kinetic rate of MB dye catalyzed by TiO_2 + MC composite with pH values of 5, 7, and 10 is 0.001 min^{-1}, 0.004 min^{-1}, and 0.006 min^{-1}.

The charge separation efficiency was the study of the TiO_2 nanoflower thin film by many test procedures using photoelectrochemical cells. Liner sweep

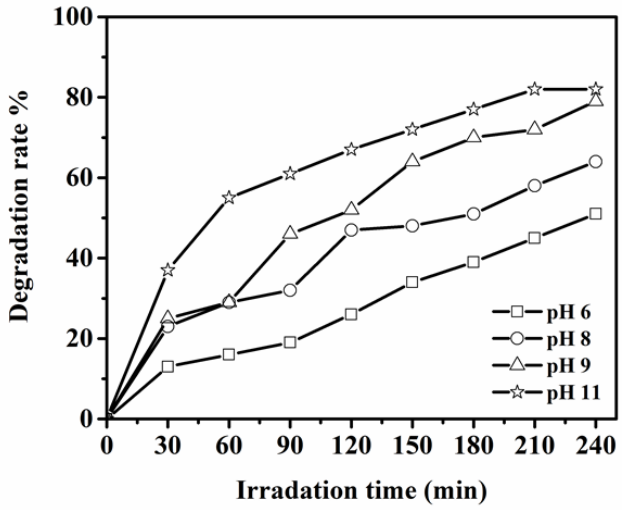

Fig.7. MB dye photodegradation rate vs. irradiation time for MB dye treated by TiO_2 nanoflowers thin film using various value of pH.

Table 1. Approach for using TiO_2 nanostructures in prior studies by using different measurement parameters.

TiO_2 structure	Time Irradiation (min)	Dye	Degradation rate %	pH	Source	Reference
uniformly acquired by nearly spherical	540	congo red	14	6.53	visible light	[31]
TiO_2 nanoflower deposited on bauxite hollow fibre membrane	360	bisphenol A	78	--	UV	[60]
TiO_2 nanoflower	240	MB	51 64 79 82	6 8 9 11	UV	This work

Table 2. Degradation rate % and k value with irradiation time for different pH values and irradiation duration of TiO_2 nanoflowers thin films.

	Degradation rate%								K
pH	30min	60min	90min	120min	150min	180min	210min	240min	min^{-1}
6	13	16	19	26	34	39	45	51	0.0028
8	23	29	32	47	48	51	58	64	0.0038
9	25	29	46	52	64	70	72	79	0.0061
11	37	55	61	67	72	77	82	82	0.0069

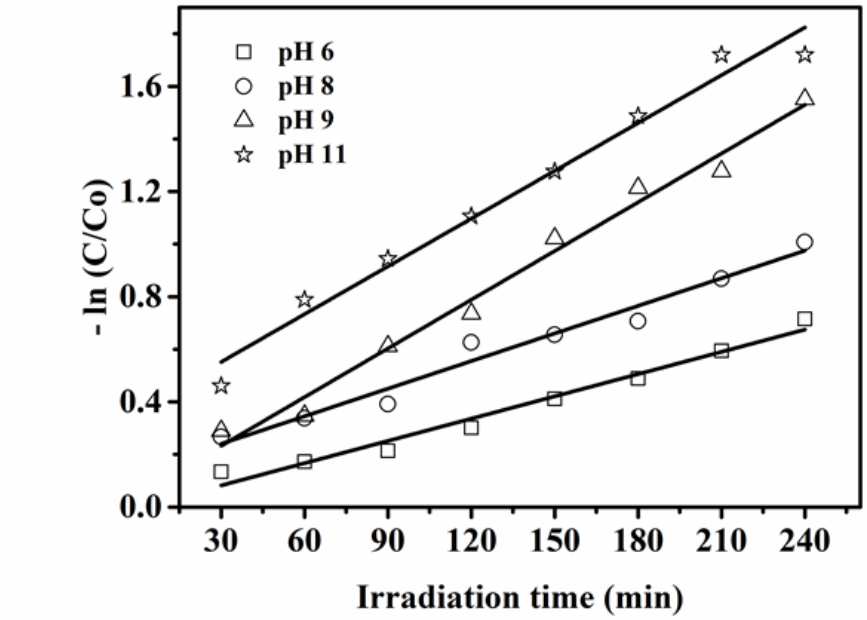

Fig.8. Variation of −ln (C/C_o) vs. irradiation time for different pH values for TiO_2 nanoflowers thin film using various value of pH.

Voltammetry (LSV) measurement was performed separation charge with 1M of KOH solution under 0.05 V s^{-1} scan rate as shown in **Fig. 9A** which response sample under UV irradiation and noted positive photocurrent response induced under ultraviolet effect. Photocurrents at 0.1 V under dark, and UV are 0.133, and 0.149 $mAcm^{-2}$ respectively. Impedance spectroscopy (EIS) of TiO_2 nanoflower each dark and UV irradiation as shown in **Fig. 9B**, and noted an intercept at high frequency for the electrolyte resistance Re on the intersection with the axis real axis Z', followed by an inclined line begins with 50118.72 Hz to the low-frequency range to 0.1 Hz which is corresponding Z" (0.096 to $8.064x10^3$) Ohm for dark and (0.103 to $7.753x10^3$) Ohm for UV in case of inclined line, the impedance spectrum is likely to be the shape of a Warburg semi-infinite [57]. The slanted line can be caused by ion diffusion into the material electrode, a process known as Warburg diffusion [58]. Resistance Warburg (W1) was the estimated value from the circle equivalent which equals 105.48 Ω while resistance photoelectrode (R1) is 3.33 Ω, and resistance charge transfer (R2) is 2.19 Ω. **Fig. 9C** shows the cycle voltammetry test of the TiO_2 nanoflower thin film and displays non-faradic capacitance behavior and the absence of beaks of redaction and oxidation. The reason the return of the thin film is rapidly charged and discharged using the perfect voltammetric at a rate semi-constant, good electrical conductivity, redox sites are electrically connected, reversibility and quick reactivity for redox processes, separations of a brief lifetime, and avoid solid ion diffusion by providing the majority of the location on the surface [59].

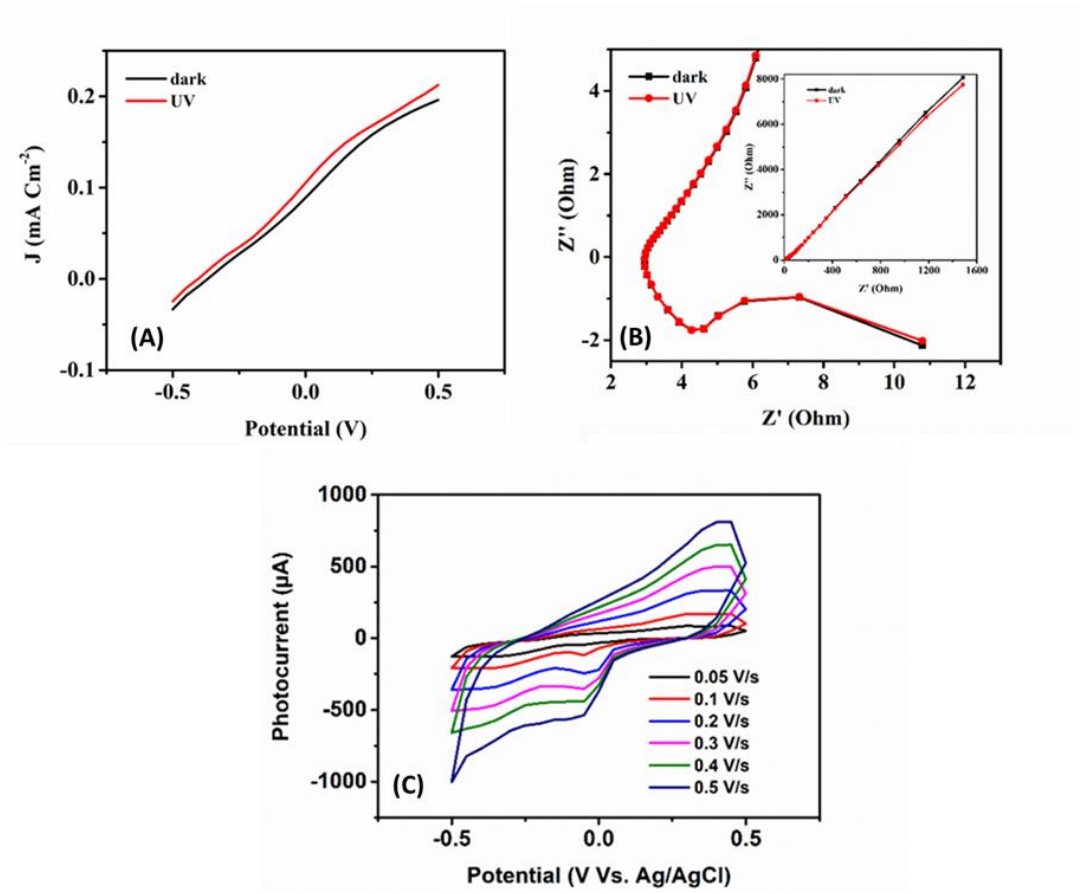

Fig. 9. (A) LSV (B) EIS plot (C) CV of the TiO_2 nanoflower thin film.

4. Conclusions

The CBD technique is used to prepare the TiO_2 nanoflower thin films onto glass substrates. The energy band gap of the synthesized TiO_2 nanoflower thin films was 3.26 eV and they had an anatase phase structure. With different pH levels and UV light irradiation periods, the photodegradation of TiO_2 nanoflower thin films for MB dye is studied. The findings indicate that increasing the pH value and the irradiation period enhanced the photodegradation rate of MB dye. After 240 minutes of exposure, the photodegradation rates of the MB dye were 51%, 64%, 79%, and 82% for the pH values of 6, 8, 9, and 11, respectively. This behavior can be linked to increased OH concentrations, which function as strong oxidation sites with photogenerated holes, resulting in MB dye photodegradation. Furthermore, the nanoflower structure of TiO_2 aids in photodegradation by increasing the interaction area between TiO_2 and MB dye solution. Furthermore, the photodegradation process is evaluated by the first-order Langmuir relation. Photocatalytic degradation of MB dye was achieved with kinetic rate constants of 0.0069, 0.0061, 0.0038, and 0.0028 min^{-1} for pH values of 11, 9, 8, and 6, respectively.

Acknowledgements

The authors acknowledge Department of Physics-College of Science- University of Basrah for suporting the work.

References

[1] A. P. Vieira, S. A.A. Santana, C. W.B. Bezerra, H. A.S. Silva, J. A.P. Chaves, J. C.P. Melo, E. C. S. Filho, C. Airoldi , *Chem. Engin. J.*, 173(2011) 334–340.

[2] A. R. Khataee, M. Zarei, L. Moradkhannejhad, *Desalination*, 258(2010) 112–119.

[3] K. A. Isai, V. S. Shrivastava, *Iran. J. Catal*., 9 (2019) 259-268

[4]M. Shabir, M.Yasin, M. Hussain, I. Shafiq, P. Akhte r, A-S. Nizami, B-H. Jeon, Y-K. Park, *J. Indus. Engin. Chem.*, 112 (2022) 1–19.

[5] S. A. Mirsalari, A. Nezamzadeh-Ejhieh, A. R. Massah, *Envir. Sci. and Poll. Res.*,29 (2022), 33013–33032.

[6]Z. Mengting, T. A. Kurniawan, S. Fei, T. Ouyang, M. Hafiz, D. Othman, M. Rezakazemi, S. Shirazian, *Envir. Poll.*, 255 (2019) 113182.

[7] M. Ghaedi, A. M. Ghaedi, M. Hossainpour, A. Ansari, M. H. Habibi, A. R. Asghari, *Jour. Ind. and Engin. Chem.*, 20 (2014), 1641–1649.

[8] G. Zhu, X. Xing, J. Wang, X. Zhang, *J. Mater. Sci.*, 52(2017) 7664–7676.

[9] A. Rostami-Vartooni, A. Moradi-Saadatmand, M. Bagherzadeh, M. Mahdavi, *Iran. J. Catal.*, 9(2019), 27-35.

[10] M. Arunkumar, A. S. Nesaraj, Iran. J. Catal., 10(2020) 235-245.

[11] M. Zebardast, A. Fallah Shojaei, K. Tabatabaeian, Iran. J. Catal., 8(2018), 297-309.

[12] K. H. Rahman, A. K. Kar, *J. Environ. Chem. Eng.*, 8(2020) 104181, 2020.

[13] R. Daghrir, P. Drogui, R. Didier, *Ind. Eng. Chem. Res.*, 52(2013), 3581–3599.

[14] S. Rajagopal, B. Paramasivam, K. Muniyasamy, *Sep. Purif. Technol.*, 252(2020), 117444.

[15] H. Derikvandi, A. Nezamzadeh-Ejhieh, *J. Hazard Mater.*, 321(2017), 629–638.

[16] N. Arabpour, A. Nezamzadeh-Ejhieh, *Pro. Safe. and Envir. Prote.*, 102(2016) 431–440.

[17] Y. Deng, R. Zhao, *Curr. Poll. Rep.*,1(2015), 167–176.

[18] H. Li, Y. Zhou, W. Tu, J. Ye, Z. Zou, *Adv. Funct. Mater*, 25(2015), 998–1013.

[19] M. J. Kadhim, M. A. Mahdi, J. J. Hassan, *mate. Inter.*, 2(2020), 0064–0072.

[20] D. Sánchez-Martínez, A. Martínez-De La Cruz, E. López-Cuéllar, *Mater. Res. Bull.*, 48(2013) 691–697.

[21]X. Liu, M. Sayed, C. Bie, B. Cheng, B. Hu, J. Yu, L. Zhang , *J. Mate.*, 7 (2021), 419–439.

[22] H. Tran Thi Thuong, C. Tran Thi Kim, L. Nguyen Quang, H. Kosslick, *Prog. in Natu. Scie.: Mater. Inter.*, 29(2019), 641–647.

[23] R. P. Souza, E. Ambrosio, M. T. F. Souza, T. K. F. S. Freitas, A. M. Ferrari-Lima, J. C. Garcia, *Envir. Scie. and Poll. Res.*, 24(2017), 12691–12699.

[24] E. Cerrato, E. Gaggero, P. Calza, M. C. Paganini, *Chem. Eng. J. Adv.*, 10(2022) 100268.

[25] W. Li, R. Liang, A. Hu, Z. Huang, Y. N. Zhou, *RSC Adv.*, 4(2014) 36959–36966.

[26] A. Yousefi, A. Nezamzadeh-Ejhieh, *Iran. J. Catal.*, 11(2021) 247-259.

[27] A. Nezamzadeh-Ejhieh, M. Khorsandi, *J. Hazard Mater.*, 176(2010), 629–637.

[28] A. M. Selman, Z. Hassan, M. Husham, *Measurement*, 56(2014), 155–162.

[29] M. J. Kadhim, F. Allawi, M. A. Mahdi, S. N. Abaas, *Iran. J. Mater. Scie. and Engin.*, 19(2022) 1–15.

[30] M. A. Mahdi, S. J. Kasem, J. J. Hassen, A. A. Swadi, S. K. J. Al-Ani, *International*, 2(2009), 163–172.

[31] K. B. Chaudhari, Y. N. Rane, D. A. Shende, N. M. Gosavi, S. R. Gosavi, *Optik*, 193(2019) 163006.

[32] A. H. Mayabadi, V. S. Waman, M. M. Kamble, S. S. Ghosh, B. B. Gabhale, S. R. Rondiya, A. V. Rokade, S. S. Khadtare, V. G. Sathe, H. M. Pathan, S. W. Gosavi, S. R. Jadkar, *J. Phy. and Chem. Solids*, 75 (2014), 182–187.

[33] T. A. Kurniawan, Z. Mengting, D. Fu, S. K. Yeap, M. Hafiz, D. Othman, R. Avtar, T. Ouyang, *J. Environ. Manage.*, 270(2020) 110871.

[34] M. Sharma, K. Behl, S. Nigam, M. Joshi, *Vacuum*, 156(2018) 434–439.

[35] M. J. Kadhim, M. Mahdi, J. J. J. Hassan, A. S. Al-Asadi, *Nanotechnology*, 32(2021) 195706.

[36] A. M. Selman, M. J. Kadhim, *Opt. Mater.* , 131(2022) 112664.

[37] S. Dharmraj Khairnar, R. Patil, V. S. Shrivastava, Iran. J. Catal. 8 (2018) 143-150.

[38] M. A. Mahdi, Z. Hassan, S. S. Ng, J. J. Hassan, S. K. M. Bakhori, *Thin Solid Films*, 520(2012), 3477–3484.

[39] P. Makuła, M. Pacia, W. Macyk, *J. Phy. Chem. Lett.*, 9(2018) 6814–6817.

[40] S. A. Mirsalari, A. Nezamzadeh-Ejhieh, *Sep. Purif. Technol.*, 250(2020) 117235 .

[41] B. Manikandan, K. R. Murali, R. John, *Iran. J. Catal.*, 11(1), 2021, 1-11

[42] S. Dianat, Iran. J. Catal. 8(2018) 121-132 .

[43] J. M. Kalita, M. P. Sarma, G. Wary, *Thin Solid Films*, 726(2021) 138656

[44] A. Nezamzadeh-Ejhieh, M. Karimi-Shamsabadi, *Chemical Engineering Journal*, 228(2013), 631–641.

[45] S. Senobari, A. Nezamzadeh-Ejhieh, *J. Mol. Liq.*, 257(2018), 173–183.

[46] K. Murugan, J. Joardar, A. S. Gandhi, B. S. Murty, P. H. Borse, *RSC Adv.*, 6(2016), 43563–43573.

[47] R. Saravanan, E. Thirumal, V. K. Gupta, V. Narayanan, Ajj. Stephen, *J. Mol. Liq.*, 177(2013) 394–401.

[48] X. Nie, S. Zhuo, G. Maeng, K. Sohlberg, *Inter. J. Photo.*, 2009(2009) 22.

[49] S. S. Al-shamali, *Aust. J. Basic Appl. Sci.*, 7(2013) 172–176.

[50] S. Ghattavi, A. Nezamzadeh-Ejhieh, *J. Mol. Liq.*, 322(2021) 114563.

[51] V. Kumari, S. Sharma, A. Sharma, K. Kumari, N. Kumar, *J. Mater. Scien.: Mater. in Electr.*, 32(2021) 9596–9610.

[52] M.I.A. Abdel Maksoud, G. S. El-Sayyad, A. M. El-Khawaga, M. Abd Elkodous, A. Abokhadra, M. A. Elsayed, M. Gobara, L.I. Soliman, H.H. El-Bahnasawy, A.H. Ashour, *J. Hazard Mater.*, 3894 (2020), 123000.

[53] A. Eslami, A. Oghazyan, M. Sarafraz, *Iran. J. Catal.* 8(2018) 95-102.

[54] E. Abbasi, M. Haghighi, R. Shokrani, M. Shabani, *Mater. Res. Bull.*, 129(2020) 110880.

[55] X. Li, Y. Hou, Q. Zhao, L. Wang, *J. Colloid Interface Sci.*, 358(2011) 102–108.

[56] A. Noruozi, A. Nezamzadeh-Ejhieh, *Chem. Phys. Lett.*, 752(2020) 137587.

[57] T. Q. Nguyen, C. Breitkopf, *J. Electrochem Soc.*, 165(2018) E826–E831.

[58] Y. Cui, X. Zhao, R. Guo, *Mater. Res. Bull.*, 45(2010) 844–849.

[59] A. S. Al-Asadi, L. A. Henley, M. Wasala, B. Muchharla, N. Perea-Lopez, V. Carozo, Z. Lin, M. Terrones, K. Mondal, K. Kordas, S. Talapatra, *J. Appl. Phys.*, 121(2017), 124303.

[60] X. Wang, Y. Tang, M. Leiw, T. Lim, *Appl. Catal. A Gen.*, 409–410(2011), 257–266.